Imaging ion-molecule reactions: Charge transfer and C-N bond formation in the C$^+$ + NH$_3$ system

Linsen Pei and James M. Farrar[a)]
Department of Chemistry, University of Rochester, Rochester, New York 14627, USA

The velocity mapping ion imaging method is applied to the ion-molecule reactions occurring between C$^+$ and NH$_3$. The velocity space images are collected over the relative collision energy range from 1.5 to 3.3 eV, allowing both product kinetic energy distributions and angular distributions to be obtained from the data. The charge transfer process appears to be direct, dominated by long-range electron transfer that results in minimal deflection of the products. The product kinetic energy distributions are consistent with a process dominated by energy resonance. The kinetic energy distributions for C-N bond formation appear to scale with the total available energy, providing strong evidence that energy in the [CNH$_3$]$^+$ precursor to products is distributed statistically. The angular distributions for C-N bond formation show pronounced forward-backward symmetry, as expected for a complex that resembles a prolate symmetric top decaying along its symmetry axis. © *2012 American Institute of Physics*. [http://dx.doi.org/10.1063/1.4719808]

I. INTRODUCTION

The study of the reactions of gas phase ions with neutral species, especially stable atoms and molecules, is a subject with a long history, dating back to the origins of mass spectrometry.[1] Ionic reactions have played a central role not only in applications such as radiation chemistry,[2] semiconductor plasmas,[3] and planetary atmospheres[4] but also in fundamental studies of chemical reactivity. The earliest studies of how energy placed in specific reactant degrees of freedom controls reaction rates and the disposal of energy in the products were carried out in ionic systems.[5] Kinetic measurements have demonstrated that ion-neutral reactions are among the fastest gas phase processes known.[6] The related question of how energy is utilized in such reactions is important in the modeling of complex systems of coupled and consecutive reactions associated with the applications noted above, as well as providing experimental benchmarks for theoretical methods that predict state to state reaction cross sections.

Probing the partitioning of energy in elementary reactions is a topic that has been at the heart of the field of chemical reaction dynamics for several decades.[7] The requirement that the nascent products of such reactions be probed under single collision conditions has led to the development of a number of powerful techniques.[8] The crossed beam method provides an ideal environment for examining single-collision reactive processes in general, and ion-neutral processes in particular, providing data that complement rate constant determinations. Crossed beam experiments may be implemented in a number of ways, and a "traditional" experiment consists of product velocity or energy distributions over a range of laboratory scattering angles such that the velocity space center of mass energy and angular distributions can be extracted from the data set. In any given time interval, the detector registers a single velocity space element. Since a complete representation of the center of mass cross section may require the determination of hundreds or even thousands of velocity space intensities, the method is limited in scope.
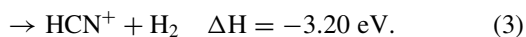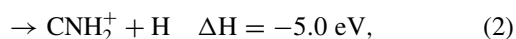
The addition of product ion imaging detection to the crossed beam method,[9] allowing all elements of product velocity space to be probed in a single time window, has made significant inroads in the field of photodissociation and in bimolecular collision processes[10] with neutral species, but application to ionic interactions is much more limited, and only two research groups have published velocity space product distributions. Weisshaar and co-workers[11] presented an early, groundbreaking study of reactions of Co$^+$ with propane and butane in which the velocity space images of the products resulting from hydrogen atom and methyl group elimination were determined. Wester and co-workers have presented studies of charge transfer between Ar$^+$ and N$_2$ (Ref. 12) and the nucleophilic substitution reaction of Cl$^-$ with CH$_3$I (Ref. 13) that provide velocity map images yielding new mechanistic insights.

In this paper, we report first results from a new imaging instrument in our laboratory. The reactions of C$^+$ with NH$_3$ provide a particularly appealing system to study via velocity map imaging,[14] owing to the existence of two kinematically distinct reactive channels accessible at low collision energies. The presence of significant concentrations of the carbon cation in diffuse atomic and molecular clouds and translucent clouds has focused attention on the role of this species in interstellar molecule formation, and numerous rate measurements of its reactions have been carried out.[15] Collisions of C$^+$ with NH$_3$ therefore not only inform studies of interstellar chemistry but also provide a demonstration of the capabilities of the velocity mapping method in ion chemistry.

Thermal rate measurements, summarized by Martinez *et al.*[15] show that the overall rate of C$^+$ destruction is over

---

a)Author to whom correspondence should be addressed. Electronic mail: farrar@chem.rochester.edu.

10^{-9} cm^3 s^{-1} and that the dominant reactions are shown below:

$$C^+ + NH_3 \rightarrow C + NH_3^+ \quad \Delta H = -1.19 \text{ eV}, \quad (1)$$

$$\rightarrow CNH_2^+ + H \quad \Delta H = -5.0 \text{ eV}, \quad (2)$$

$$\rightarrow HCN^+ + H_2 \quad \Delta H = -3.20 \text{ eV}. \quad (3)$$

Reaction (3) is clearly a minor channel, accounting for only a few percent of the total C$^+$ destruction, with charge transfer (1) contributing 25%–30% of the total rate.

II. EXPERIMENTAL

The experimental apparatus is a major modification of the crossed beam instrument that has been described in the literature.[16] In the present experiment, ions for the primary ion beam are produced with the electron impact source described by Udseth, Gentry, and Giese,[17] using a mixture of 10% CO in He. The primary product of electron impact of this mixture is He$^+$, which then reacts with CO to form ground state C$^+$ (^{2}P) cations by dissociative charge transfer.[18] Following extraction, the ions are accelerated to 300 eV and are then mass-selected by a 60° magnetic sector. After deceleration to the desired beam energy and focusing by a series of ion optics, the continuous beam of ions is delivered to the volume defined by the repeller and extraction electrodes of a velocity mapped imaging detector, the operation of which is described below. Following the interaction region, the total ion current of the ion beam can be measured, or the ion beam can be energy-analyzed by a 90° spherical sector electrostatic energy analyzer. The analyzer is the same one employed in previous studies from our laboratory[16] and is well characterized and calibrated. The beam has a roughly triangular kinetic energy distribution with a FWHM of ∼0.20 eV in the laboratory frame of reference. Experiments were performed at four relative energies from 1.5 to 3.3 eV, employing ion beam energies ranging from 2.0 to 5.5 eV. This study extends earlier work from our laboratory[19] in which the C-N bond formation process was examined at a single collision energy near 2 eV.

The neutral beam is produced by a pulsed solenoid valve located 10 mm upstream from an electroformed skimmer (Beam Dynamics). The stagnation pressure of the gas behind the 0.1 mm diameter nozzle is 3 atm. The nozzle chamber is pumped by a 25 cm diameter oil diffusion pump, maintaining a pressure of ∼3 × 10^{-6} torr during operation at a repetition rate of 10 Hz. The beam is injected directly in the main chamber, pumped by a 15 cm diameter oil diffusion pump, which maintains a pressure of ∼1 × 10^{-6} torr with the beams running. The total volume defined by the crossing of the ion and neutral beams is estimated to be a cube ∼3–5 mm on a side.

Product detection was achieved by velocity map imaging,[14] ideally suited to the crossed beam geometry, because the method focuses ions of a given mass with the same (V_x, V_y) velocity components to a single image point, irrespective of the location of an ion within the collision volume.

The method therefore removes the effect of the finite collision volume in planes parallel to the imaging plane, but does not remove the chromatic aberration that arises from the finite thickness of the collision volume perpendicular to the imaging plane.

The ion and neutral beams cross in a field free region of space in a specific time interval, but because the reactants and products are charged, velocity mapping must be initiated by pulsed electric fields applied to the collision volume after reaction has taken place. The extraction pulse is synchronized to the arrival of the central portion of the pulsed molecular beam and has a rise time of 25 ns, fast enough for the reaction products to move only small fraction of a mm. The duration of the pulse is sufficient for all charged products to leave the volume between the repeller and extraction electrodes before turning off. In practice, the pulse must be 1–2 μs long to achieve this condition.

The electrode configuration in this experiment is equivalent to the two-electrode version described by Suits et al.[20] To achieve delayed pulsed extraction, the voltage on the repeller plate, V_1, located 10 mm below the collision center, is typically pulsed to +1000 V, although the precise value depends on transverse velocity and the desired filling factor for the MCP detector. The voltage V_2 on the extraction electrode, placed 10 mm above the collision center, is pulsed to a value $V_2 = 0.64 V_1$. In conjunction with a grounded electrode placed 13 mm above the extraction electrode, this lens configuration provides velocity mapping for the product ions at the imaging plane, located 0.6 m downstream from the grounded lens.

The imaging plane of the detector is defined by the front face of a pair of chevron-mounted microchannel plates (Photonis USA, Inc), held at −1900 V. A grounded grid precedes the MCPs. The MCPs are gated by a 50 ns pulse, which is timed to allow an equatorial slice of the product ion cloud to be recorded by the phosphor screen following the MCP anode. The light image from the phosphor screen, which is held at a potential of +4000 V, is recorded by a CCD camera, which transfers the image via a USB interface to a lab computer controlled by a LabVIEW program. A typical image represents the accumulation of 5000–20 000 repetitions of the pulsed valve. All high voltage pulses are provided by commercial pulse generators (DEI PVX-4140, 4150). The drift space and imaging detector are in a separate chamber pumped by a turbomolecular pump (Pfeiffer Balzers).

Calibration in a velocity mapping experiment requires care, since the method impresses an unknown magnification on the spatial image recovered at the detector. The experiments reported here rely on direct energy analysis for the determination of the primary ion beam velocity, and collision kinematics for establishing a marker at low velocity that establishes the neutral beam velocity scale. The kinematics of resonant charge transfer between an atomic beam of Ar$^+$ and a neutral beam of Ar produced by supersonic expansion require that an Ar$^+$ signal occurring at precisely the velocity of the neutral Ar beam be detected at 90° in the laboratory coordinate system.[21] In the present experiment, a supersonic expansion of Ar at a stagnation pressure of 1 atm produces a beam with a most probable speed of $(5 kT/m)^{1/2}$ or 5.54

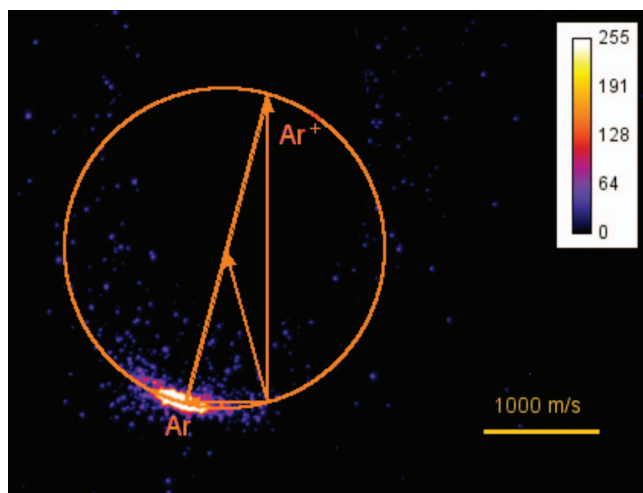FIG. 1. Ar^+ + Ar thermal charge transfer image used for calibration. The image is superimposed on the most probable Newton kinematic diagram. The tip of the Ar neutral beam corresponds to a velocity of 5.54×10^2 m s^{-1}.

$\times 10^2$ m s^{-1} under our operating conditions, corresponding to a lab energy of 0.064 eV. Figure 1 shows the Ar^+ signal produced by charge transfer at a collision energy of 1.3 eV; the position of this image is dependent only on the velocity of the neutral beam. The sharpness of the image is illustrative of the quality of experimental data that this implementation of delayed extraction provides. The quality of the image allows us to establish the accuracy and precision of the image velocities to within $\pm 0.2 \times 10^2$ m s^{-1}.

Several experimental factors contribute to the resolution of the raw images. The velocity spreads in the ion and neutral beams result in a 10% width in the initial relative velocity distributions. The finite width of the equatorial slicing pulse also contributes to the broadening of the velocity space image. For example, the charge transfer products formed at a collision energy of 2 eV define a sphere in velocity space with a radius of 3 mm/μs. The transit time of the products to the imaging plane is ~5 μs, producing a sphere of diameter 30 mm. The 50 ns slicing pulse results in an equatorial slice of width 5 mm, ~15% of the sphere diameter. Products at the upper and lower edges of the slice have speeds ~1.5%–2% smaller than the product speed at the equator. Thus, the image aberrations arising from the finite slicing pulse are small. The largest experimental factor contributing to experimental resolution comes from the finite thickness of the collision volume. Reaction products formed at various depths within the collision volume are accelerated to different extents and therefore do not satisfy a unique velocity-mapping condition. SIMION calculations suggest that this effect is comparable to the velocity broadening of the beams, and studies to investigate this factor quantitatively are underway in our laboratory.

III. RESULTS AND ANALYSIS

Figure 2 shows velocity space images for the NH_3^+ charge transfer products and the $HCNH^+/H_2CN^+$ condensation products at all collision energies. Mass resolution is insufficient to resolve the individual condensation products

from one another; extant studies[15] suggest that the dominant condensation product is H_2CN^+, and the discussion of this paper will be based on that assumption. The charge transfer image is centered at the position of the neutral beam, indicative of a process that occurs primarily through energy resonance, in which the initial kinetic energy of NH_3 and the product kinetic energy of NH_3^+ are essentially equal. In the vicinity of energy resonance, the Franck-Condon factors are consistent with the formation of NH_3^+ in a sequence of bending vibrations.[22,23] The condensation products are distributed symmetrically about the centroid of the collision system, consistent with their formation from a collision complex that lives at least several rotational periods.

The images represent product ion flux in laboratory Cartesian coordinates,[24] and a simple translation to the center of mass yields barycentric distributions in Cartesian coordinates, symbolized by $P(u_x, u_y)$. Barycentric recoil speed and scattering angle are given by the following expressions:

$$u = \left(u_x^2 + u_y^2\right)^{1/2}, \qquad (4)$$

$$\theta = \tan^{-1}(u_y/u_x). \qquad (5)$$

The relationship between Cartesian and polar flux intensity is given by the following expression:

$$I_{c.m.}(u, \theta) = u^2 P(u_x, u_y). \qquad (6)$$

Product angular and kinetic energy distributions, computed by averaging the flux distribution over recoil speed and scattering angle respectively, and denoted by the bracket notation below, require integration over the Cartesian flux. The angle-averaged relative translational energy distribution of products, $P(E_T')$, is given by the following expression:

$$\langle P(E_T') \rangle_\theta = \int_0^\pi d\theta \, \sin\theta \, u \, P(u_x, u_y). \qquad (7)$$

Integration over specific angular regions provides a means to assess how energy disposal may depend on scattering angle. Even in the case of a collision complex that lives at least several rotational periods, one might expect the angular distribution to be coupled to the recoil energy distribution, especially when hydrogen atoms are ejected, but the quality of the data reported here are insufficient to justify such an analysis.

The speed-averaged angular distribution is computed as follows:

$$\langle g(\theta) \rangle_u = \int_0^\infty du \, u^2 P(u_x, u_y). \qquad (8)$$

The total energy accessible to the reaction products is defined as

$$E_{total} = E_T + E_{int} - \Delta H, \qquad (9)$$

where E_T is the initial relative kinetic energy, E_{int} is the total internal energy of the reactants, and ΔH is reaction exoergicity. Ion production results in ground state C^+ reactants, and the neutral beam is produced by supersonic expansion, forming cold NH_3 molecules.
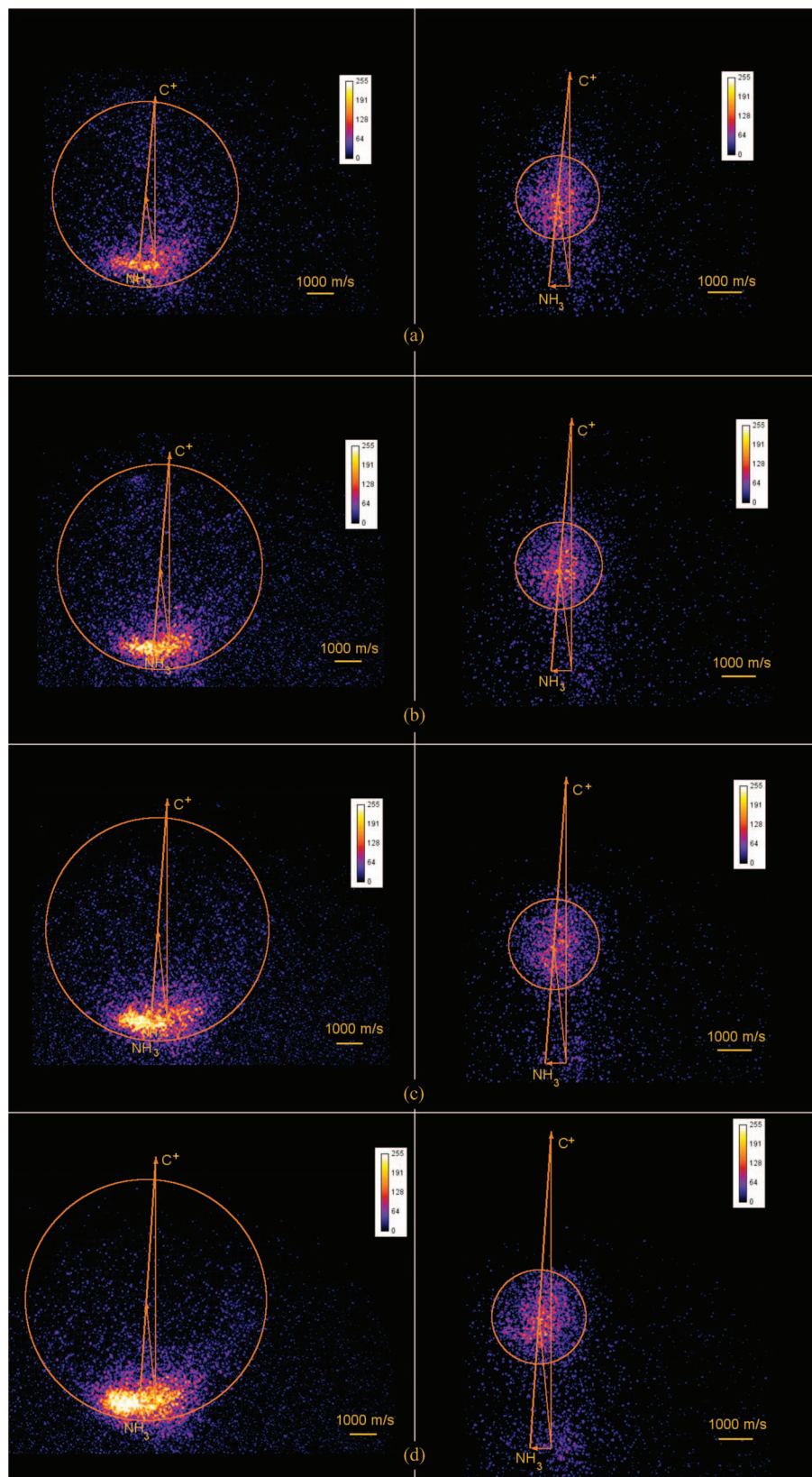
FIG. 2. Ion images for charge transfer and C-N bond formation, superimposed on the most probable Newton diagrams at a given collision energy. The left column of images corresponds to the formation of NH_3^+ by charge transfer. The right column of images corresponds to the formation of $HCNH^+$ products by C-N bond formation. The circles denote the loci of center of mass speeds that correspond to the maximum product values allowed by energy conservation. (a) $E_{rel} = 1.5$ eV; (b) $E_{rel} = 2.1$ eV; (c) $E_{rel} = 2.5$ eV; (d) $E_{rel} = 3.3$ eV.
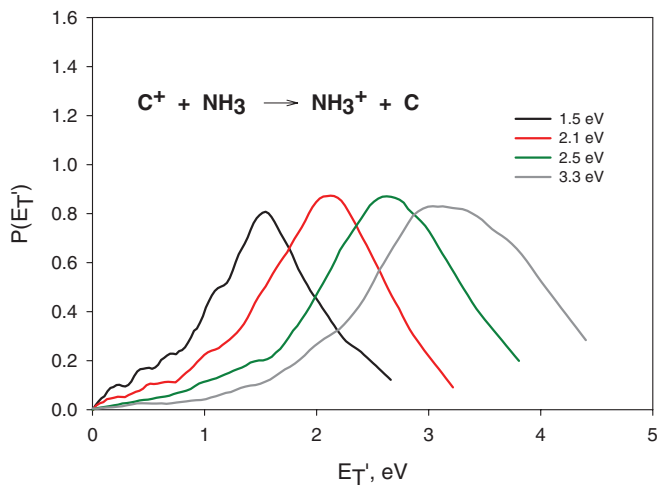
FIG. 3. Charge transfer center of mass kinetic energy distributions for four collision energies as indicated.

Figure 3 shows the kinetic energy distributions for charge transfer. The results are plotted as a function of E_T', since the energy resonance condition in which $E_T' = E_T$ is a useful benchmark for charge transfer.[25] In the vicinity of energy resonance, NH_3^+ products have ∼1 eV of vibrational excitation. The photoelectron spectrum of NH_3 consists of a broad progression of resonances corresponding to excitation of the umbrella-bending mode.[23] The spectrum, which reflects the Franck-Condon factors for ionization, peaks at $\nu_2 = 6$, or ∼0.8 eV of internal excitation, and is quite symmetric with respect to the maximum. The product kinetic energy distributions shown in Figure 3 are reasonably symmetric with respect to their maxima, and with widths that range from ∼1 to 1.5 eV, exhibit a striking resemblance to the Franck-Condon profile of the photoelectron spectrum.

The kinetic energy distributions for the C-N condensation reaction are plotted in Figure 4 as functions of f_T', the fraction of the total energy that appears in product translation. This representation is especially useful in assessing the role
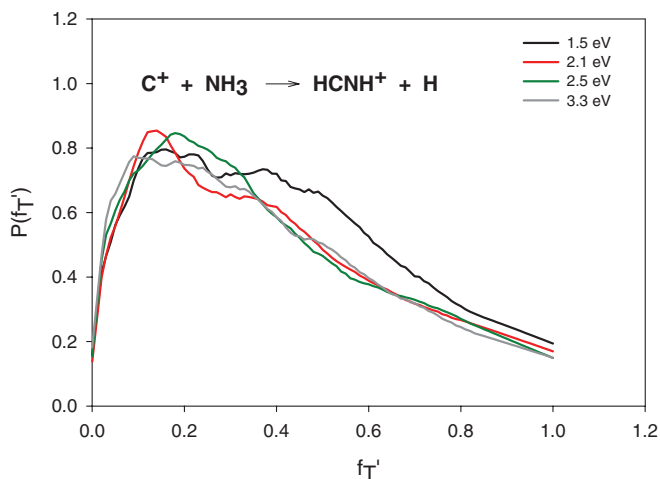

FIG. 4. C-N bond formation center of mass kinetic energy distributions, for four collision energies as indicated. Horizontal axis is f_T', the fraction of the total energy in product translation.

TABLE I. Product branching fractions.

Collision energy (eV)	Fractional yield, charge transfer
0.02 (thermal) (Ref. 15)	0.28
1.5	0.81
2.1	0.86
2.7	0.91
3.3	0.93

of the total available energy, as contrasted with energy in particular internal energy states of the reactants, in controlling product energy partitioning. The distributions are essentially superimposable over the full range of initial kinetic energies, suggestive of an underlying statistical mechanism for energy partitioning.[26]

It is straightforward to extract branching ratio data from the measured images. Those data are presented in Table I, along with the value reported in thermal energy flow tube studies.[15] The charge transfer process represents only 30% of the product at thermal energy but becomes the dominant product in the higher energy range of these experiments. The energy dependence of the branching ratio reflects dynamics on two different parts of the potential energy surface. Charge transfer reflects couplings at large distances between two surfaces associated with two different arrangements of charge. The C-N bond formation channel reflects the energy dependence of formation of a transient complex in which all atoms are strongly interacting, a process for which the cross section decreases with increasing energy.

IV. DISCUSSION

This study extends the results of our prior work, in which the C-N bond formation reaction only was studied at a collision energy of 2 eV, both to lower and higher collision energies, and provides new data on the charge transfer process. The kinetic energy distribution measured at 2.1 eV is in good agreement with the results reported in our original study.[19] In that study, we were able to distinguish between the formation of $HCNH^+ + H$ and $HCN^+ + H_2$, the latter channel of significantly lower intensity than the former, but the mass resolution in the present geometry is insufficient to distinguish the channels. The $HCNH^+$ channel is 1.8 eV more exoergic, and reaction products are formed all the way to this limit, observations that are consistent with predominant formation of this product.

Ab initio calculations[27] have predicted that insertion of C^+ into an N-H bond of NH_3 forms a complex that is stable with respect to reactants by almost 7 eV. Hydrogen migration in this complex appears to favor the formation of a nonclassical cation in which two hydrogen atoms are bound to the nitrogen atom and one to carbon. The present experimental data are unable to provide additional insight into the structure of the intermediate, but the scaling of the kinetic energy distributions that characterize hydrogen atom emission with total energy provides strong evidence that the decay is statistical.

The angular distributions for product formation, shown in Figure 5, exhibit the symmetry about 90° in the center of
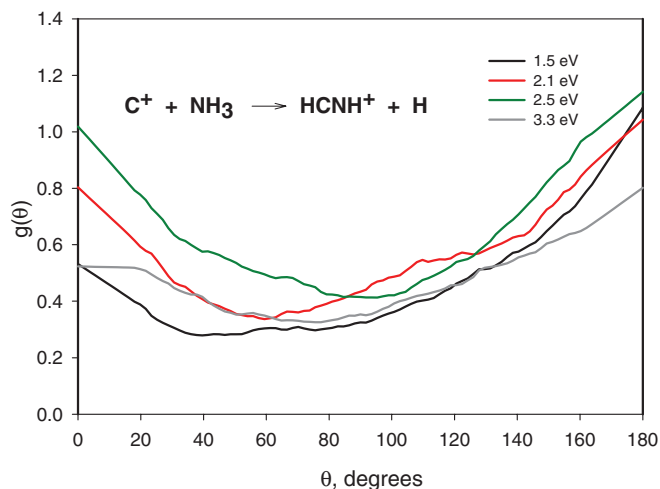
FIG. 5. Center of mass angular distributions for C-N bond formation products at four collision energies as indicated.

mass system that is expected for decay of a transient complex that lives at least several rotational periods.[28] The distinct peaks that occur at 0° and 180° are consistent with the decay of a prolate complex decaying along its symmetry axis. For a system with two heavy atoms, this angular distribution is the expected decay motif, and the significant scattering throughout the entire angular range is consistent with large amplitude hydrogen atom motion in the complex prior to decay.

Charge transfer data were not reported in our previous study but are readily accessible via imaging. The asymmetry of the product flux distributions with respect to the center of mass direction provides clear evidence that charge transfer is a direct process, which is not surprising, given that long-range electron transfer should not affect the momenta of the much heavier atomic and molecular collision partners. The angular distributions of the products, shown in Figure 6, are typical of charge transfer reactions, with products formed in a narrow range near 180°, the direction of travel of the neutral NH_3 precursor. Not only does electron transfer result in very small angular deflections of the reactants, but the product kinetic en-
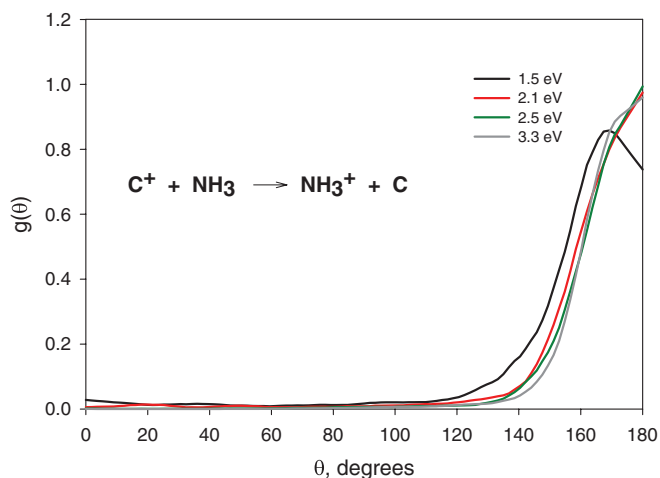
ergy distributions of Figure 3 also demonstrate that the most probable product kinetic energies are very close to the energies of the approaching reactants. However, the accessibility of NH_3^+ vibrational states with favorable Franck-Condon factors near resonance provides a mechanism for forming a range of product vibrational states, evidenced by the breadth of the kinetic energy distributions. Franck-Condon factors extracted from photoelectron spectra indicate that the most likely vibrational mode populated by electron transfer is the umbrella bending motion.[23]

V. CONCLUSIONS

This study has provided additional data on an important reaction in interstellar chemistry. Moreover, the study provides another demonstration of the value of ion-imaging experiments as a probe of energy disposal in ion-neutral reactions, especially in systems with more than a single product channel. The multiplex advantage that the method provides decreases data acquisition time, allowing systems to be studied over a broader range of kinetic energy. Given the maturity of the state of knowledge of collisions of ionic species with stable, closed-shell atoms and molecules, we believe that the imaging method has a particularly bright future in the study of reactions of ions with transient species such as free radicals. Such systems represent an area where we expect to devote significant effort.

FIG. 6. Center of mass angular distributions for charge transfer products at four collision energies as indicated.

[1] J. J. Thomson, *Rays of Positive Electricity* (Longman, Green, and Company, Essex, 1913), p. 116.
[2] B. C. Garrett, D. A. Dixon, D. M. Camaioni, D. M. Chipman, and M. A. Johnson, Chem. Rev. **105**, 355 (2005).
[3] P. B. Armentrout, Adv. At. Mol. Opt. Phys. **43**, 187 (2000).
[4] A. G. Suits, J. Phys. Chem. A **113**, 11097 (2009); D. G. Torr, Rev. Geophys. **17**, 510, doi:10.1029/RG017i004p00510 (1979).
[5] W. A. Chupka and M. E. Russell, J. Chem. Phys. **49**, 5426 (1968); **48**, 1527 (1968).
[6] Y. Ikezoe, S. Matsuoka, M. Takebe, and A. Viggiano, *Gas Phase Ion-Molecule Reaction Rate Constants Through 1986* (Maruzen, Tokyo, 1987).
[7] Y. T. Lee, Angew. Chem. Int. Ed. **26**, 939 (1987); D. R. Herschbach, *ibid.* **26**, 1221 (1987).
[8] J. M. Farrar and W. H. Saunders, Jr., *Technique for the Study of Ion-Molecule Reactions* (Wiley, New York, 1988).
[9] D. W. Chandler and P. L. Houston, J. Chem. Phys. **87**, 1445 (1987); P. L. Houston, Acc. Chem. Res. **28**, 453 (1995).
[10] M. N. R. Ashfold, N. H. Nahler, A. J. Orr-Ewing, O. P. J. Vieuxmaire, and R. L. Toomes, Phys. Chem. Chem. Phys. **8**, 26 (2006).
[11] E. L. Reichert and J. C. Weisshaar, J. Phys. Chem. A **106**, 5563 (2002); E. L. Reichert, G. Thurau, and J. C. Weisshaar, J. Chem. Phys. **117**, 653 (2002).
[12] J. Mikosch, U. Fruehling, S. Trippel, D. Schwalm, and M. Weidemueller, Phys. Chem. Chem. Phys. **8**, 2990 (2006).
[13] J. Mikosch, S. Trippel, C. Eichhorn, R. Otto, and U. Louderaj, Science **319**, 183 (2008).
[14] A. Eppink and D. H. Parker, Rev. Sci. Instrum. **68**, 3477 (1997).
[15] O. Martinez, N. B. Betts, S. M. Villano, N. Eyet, and T. P. Snow, Astrophys. J. **686**, 1486 (2008).
[16] R. M. Bilotta, F. N. Preuninger, and J. M. Farrar, J. Chem. Phys. **72**, 1583 (1980).

[17]H. Udseth, C. F. Giese, and W. R. Gentry, Phys. Rev. A **8**, 2483 (1973).

[18]R. D. Smith and J. H. Futrell, J. Chem. Phys. **65**, 2574 (1976).

[19]R. A. Curtis and J. M. Farrar, J. Chem. Phys. **84**, 127 (1986).

[20]D. Townsend, M. P. Minitti, and A. G. Suits, Rev. Sci. Instrum. **74**, 2530 (2003).

[21]M. L. Vestal, C. R. Blakley, and J. H. Futrell, Phys. Rev. A **17**, 1337 (1978).

[22]D. J. Levandier and Y. H. Chiu, J. Chem. Phys. **133**, 154304 (2010).

[23]D. Edvardsson, P. Baltzer, L. Karlsson, B. Wannberg, and D. M. P. Holland, J. Phys. B **32**, 2583 (1999).

[24]R. Wolfgang and R. J. Cross, J. Phys. Chem. **73**, 743 (1969); B. Friedrich and Z. Herman, Collect. Czech. Chem. Commun. **49**, 570 (1984).

[25]J. B. Laudenslager, W. T. Huntress, and M. T. Bowers, J. Chem. Phys. **61**, 4600 (1974).

[26]R. D. Levine and R. B. Bernstein, Acc. Chem. Res. **7**, 393 (1974).

[27]M. J. Frisch, K. Raghavachari, J. A. Pople, W. J. Bouma, and L. Radom, Chem. Phys. **75**, 323 (1983).

[28]M. K. Bullitt, C. H. Fisher, and J. L. Kinsey, J. Chem. Phys. **60**, 478 (1974); W. B. Miller, S. A. Safron, and D. R. Herschbach, Faraday Discuss. Chem. Soc. **44**, 108 (1967).